



**HAL**  
open science

## Effect of sub-surface hydrogen on intrinsic crack tip plasticity in aluminium

Yu Wang, D. Connétable, Dôme Tanguy

► **To cite this version:**

Yu Wang, D. Connétable, Dôme Tanguy. Effect of sub-surface hydrogen on intrinsic crack tip plasticity in aluminium. *Philosophical Magazine*, 2019, 99 (19), pp.2355-2375. 10.1080/14786435.2019.1624850 . hal-02392410

**HAL Id: hal-02392410**

**<https://hal.science/hal-02392410>**

Submitted on 10 Dec 2019

**HAL** is a multi-disciplinary open access archive for the deposit and dissemination of scientific research documents, whether they are published or not. The documents may come from teaching and research institutions in France or abroad, or from public or private research centers.

L'archive ouverte pluridisciplinaire **HAL**, est destinée au dépôt et à la diffusion de documents scientifiques de niveau recherche, publiés ou non, émanant des établissements d'enseignement et de recherche français ou étrangers, des laboratoires publics ou privés.

# Effect of sub-surface hydrogen on intrinsic crack tip plasticity in aluminium

Y. Wang, D. Connétable, D. Tanguy

► **To cite this version:**

Y. Wang, D. Connétable, D. Tanguy. Effect of sub-surface hydrogen on intrinsic crack tip plasticity in aluminium. *Philosophical Magazine*, Taylor & Francis, 2019, 99 (19), pp.2355-2375. 10.1080/14786435.2019.1624850 . hal-02392410

**HAL Id: hal-02392410**

**<https://hal.archives-ouvertes.fr/hal-02392410>**

Submitted on 10 Dec 2019

**HAL** is a multi-disciplinary open access archive for the deposit and dissemination of scientific research documents, whether they are published or not. The documents may come from teaching and research institutions in France or abroad, or from public or private research centers.

L'archive ouverte pluridisciplinaire **HAL**, est destinée au dépôt et à la diffusion de documents scientifiques de niveau recherche, publiés ou non, émanant des établissements d'enseignement et de recherche français ou étrangers, des laboratoires publics ou privés.

# Effect of sub-surface hydrogen on intrinsic crack tip plasticity in aluminium

Y. Wang<sup>a,b</sup>, D. Connétable<sup>b</sup> and D. Tanguy<sup>a\*</sup>

<sup>a</sup> *Université de Lyon, Université Claude Bernard Lyon 1, CNRS, Institut Lumière Matière, F-69622 Villeurbanne Cedex, France;*

<sup>b</sup> *CIRIMAT UMR 5085, CNRS-INPT-UPS, École Nationale d'Ingénieurs en Arts Chimiques et Technologiques (ENSIACET) 4, allée Émile Monso, BP 44362, F-31030 Toulouse Cedex 4, France*

## ARTICLE HISTORY

Compiled June 3, 2019

## ABSTRACT

The effects of sub-surface hydrogen and mixed mode loading on dislocation emission in aluminium are studied using a combination of techniques including: crack simulations with an empirical interatomic potential, generalised stacking fault energy (GSF) calculations, with empirical interactions and Density Functional Theory, and the model by Rice which links the critical stress intensity factor to the unstable stacking energy. The crack orientation is  $\{111\}\langle 112 \rangle$  and the loading is composed of a moderate traction along  $\langle 111 \rangle$  and a shear along  $\langle 112 \rangle$ , such that Shockley partials are emitted along the crack plane. The role of the relaxations around the H atoms and of the concentration of H in the glide plane, in the GSF calculation, are revealed by comparing Rice's model to the results of brute force simulations. The enhanced GSF is then calculated *ab initio*. The conclusion is a large decrease of the critical load to emit a dislocation, due to the displacement transverse to the glide direction. The effect of sub-surface hydrogen is negligible with respect to the mechanical one.

## 1. Introduction

Hydrogen is ubiquitous in metallic materials in service [1, 2]. When they come in contact with an aqueous medium, for example, H is produced by electrochemical reactions involving the reduction of protons coming from the dissociation of water molecules. Most of the adsorbed hydrogen  $H_{ads}$  recombines but a small fraction penetrates the lattice as interstitial atoms. Then, hydrogen interacts with crystalline defects and features of the microstructure and often degrades the material's mechanical properties. In particular, it can render a ductile material brittle. Different scenarios have been proposed to explain the physical origin of this embrittlement, such as: decohesion [3–5], intense and localised plasticity [6–9], enhanced dislocation production at the crack tip due to adsorbed hydrogen [10] and production of vacancies stabilised by hydrogen [11–13]. Some of the physical ingredients proposed in these scenarios have been tested by atomic scale simulations, such as: the loss of cohesion of grain boundaries due to a static segregation of hydrogen [14, 15] or to nanoscale cavities [16, 17], the interaction

---

\*Corresponding author. Email: dome.tanguy@univ-lyon1.fr

between dislocations and vacancy-hydrogen clusters [18, 19], or the shielding of elastic interactions between dislocations by the Cottrell atmospheres [20]. In spite of progress, a quantitative microscopic model of embrittlement has not been achieved yet.

The purpose of this paper is to contribute to the quantification of the effect of hydrogen on dislocation emission from the crack tip itself. Two recent studies [21, 22], based on the Density Functional Theory (DFT) applied at model crack tips, are reported in the literature. The configuration studied in [21] is a blunted crack in a  $\{110\}$  plane, propagating in the  $\langle 111 \rangle$  direction (crack front along  $\langle 112 \rangle$ ). It is shown that the response of the crack tip to an external load largely depends on the surface site where the H atoms are adsorbed, i.e. bridge or top, and also on how stretched the Al-Al bonds are. In bridge position, H can have no effect or slightly increase the critical load for dislocation emission  $k_{Ie}$ .  $k_{Ie}$  is the stress intensity factor for dislocation emission in mode I (traction). It represents the elastic singularity at the nano scale, in the absence of extrinsic plasticity and is typically below  $1 \text{ MPa}\sqrt{\text{m}}$  [16, 23], contrary to engineering toughness. In sub-surface position, in the glide plane, hydrogen can slightly decrease  $k_{Ie}$ . A sharper crack, along the  $\{111\}$  plane, propagating in the  $\langle 112 \rangle$  direction (crack front along  $\langle 110 \rangle$ ) is studied in [22]. In this case,  $k_{Ie}$  is increased by 26% in the presence of  $\text{H}_{ads}$ . In complement of these studies, we quantify the influence of sub-surface hydrogen, in the  $\{111\}$   $\langle 112 \rangle$  crack orientation, under mixed mode loading. The critical stress intensity factor for emission along the crack plane, in mode II, under the influence of an additional mode I loading and in the presence of a hydrogen concentration  $C_H$  in the glide plane,  $k_{IIe}(k_I, C_H)$ , is calculated. The paper is organised as follows. First, the modelling strategy and the technical details of the different methods are given. Second,  $k_{IIe}(k_I, C_H)$  values, obtained from mixed mode loading crack simulations are reported, in the pure metal case first and then in the presence of hydrogen. The values of the opening  $\Delta u_z$  at the crack tip, at the onset of dislocation emission, are calculated. Third, the effects of H and  $\Delta u_z$  on the generalised stacking fault energy (GSF) are evaluated, with empirical atomic interactions and with DFT. The analytical model by Rice [24] is used to obtain  $k_{IIe}(k_I, C_H)$  from the DFT calculations. Finally, a conclusion on the effect of sub-surface hydrogen v.s. a mechanical effect of the opening perpendicular to the glide plane is given.

## 2. Simulation and Modelling details

The modelling strategy is motivated by the need to use DFT to obtain reliable  $k_{IIe}$  values. The analytical model derived by Rice in [24] for  $k_{IIe}$  is exact when emission occurs along the crack plane. It relates  $k_{IIe}$  to the unstable stacking energy  $\gamma_{us}$  (the local maximum of the GSF in the glide direction) by

$$k_{IIe} = \sqrt{2\mu\gamma_{us}(\Delta u_z(k_I, C_H), C_H)/(1 - \nu)} \quad (1)$$

where  $\mu$  and  $\nu$  are the shear modulus and Poisson ratio of the material. Mode I can be taken into account [25, 26] provided the proper transverse opening  $\Delta u_z$  is included in the calculation of  $\gamma_{us}$ . Furthermore, including H in the GSF increases the complexity of the calculation because the neighbourhood of the H atom needs to be relaxed, while the GSF is calculated by rigidly sliding two crystal blocks one on top of the other. As a consequence, the modelling strategy involves several steps:

- Brute force Molecular Statics simulations (section 3) are performed on a system

containing an internal crack, quasi-statically loaded in mode II until dislocation emission occurs. A small mode I is superimposed.  $k_{IIe}(k_I, C_H)$  values are extracted from the stress maps calculated at the atomic scale by a fit to the elastic solutions [26]. They are used as references.

- The transverse opening  $\Delta u_z$  is extracted from the crack opening profile (section 3) when the load is immediately below the critical value, i.e. at  $k_{IIe}^-$ :

$$\Delta u_z(y) = (u_z^+ - u_z^-)(y) \quad (2)$$

where  $y$  is the position along the crack plane (Fig. 1),  $u_z^+$  (resp.  $u_z^-$ ) is the displacement in the  $z$  direction (the traction direction) of the atoms of the upper (resp. lower) plane, in first neighbour of the glide plane.

- $\Delta u_z$  is included in the calculation of the GSF from which  $\gamma_{us}$  is extracted (section 4.2). In every of these first steps, the interactions are given by the same empirical interatomic potential. Rice's model gives  $k_{IIe}$  from  $\gamma_{us}$  according to equation 1. Such  $k_{IIe}$  values are compared to the ones obtained by the crack simulations in order to validate which concentration  $C_H$ , which relaxations around the H atoms and which  $\Delta u_z$  values should be used in the GSF calculations in order to reproduce the references (the  $k_{IIe}$  from brute force QMD). Indeed, even if a full line of hydrogen is introduced in the crack simulations, its effect on  $k_{IIe}$  is not coherent with a GSF calculation with 100% coverage with hydrogen. The optimal coverage is an output of the comparison between the crack simulations and Eq. 1. Furthermore, the precise location where  $\Delta u_z$  should be measured in the crack simulation is also an output of the procedure.
- After this validation, Eq. 1 is used with  $\gamma_{us}$  values calculated from DFT (section 4.3) and conclusions are drawn about the effect of H and transverse mechanical loading on dislocation emission.

### 2.1. Crack simulation set-up

Molecular Statics is used with a single crystal Al containing an internal crack. The crack problem is schematically represented in Fig. 1. The simulation box is a thin parallelepiped whose sides are  $3,4 \text{ nm} \times 54,4 \text{ nm} \times 58,8 \text{ nm}$  defined by the axes  $x = [1\bar{1}0]$ ,  $y = [11\bar{2}]$  and  $z = [111]$ , respectively. These directions are defined in the canonical base of the fcc lattice. Periodic boundary conditions are applied in the  $x$  and  $y$  directions. The calculation is three dimensional in the fcc structure, but the dimension in  $x$  is reduced. The initial crack is introduced along the (111) plane by removing two atomic layers in the box centre. Its length  $2a$ , along the  $y$  direction, is  $6.4 \text{ nm}$  (equal to  $16 a_0$ , where  $a_0$  is the lattice parameter  $4.04 \text{ \AA}$ ). The crack length is small but large enough to define  $k_I$  and reach a good agreement with elasticity [27]. The size of the box is therefore five times larger than the crack. This is sufficient to obtain a good agreement between the stress fields calculated atomistically and the analytic solution for a crack in an infinite elastic medium, in plane strain [26]. This geometry gives, in the  $x$  direction, an infinite crack front and an infinite dislocation line if emitted. The box size is eight times the crack length in the  $z$  direction. The particles in the three upper and lower layers, in the  $z$  direction, are fixed. The mechanical load is applied by giving the upper fixed layers a displacement  $(0, U_y, U_z)$ . The mode I loading corresponds to a displacement in  $z$ ,  $U_z$  only. Mode II is a shear obtained by  $U_y$  only. A mixed mode loading is obtained by superposition of mode I and mode II.

The atomic interactions are modelled by the embedded atom method (EAM). While

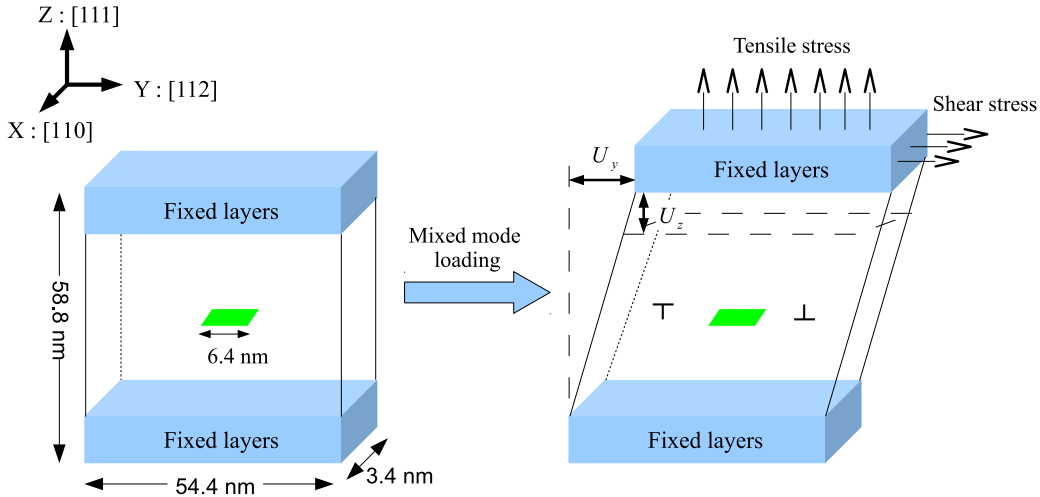


**Figure 1.** Schematic of the simulation box with an embedded crack.  $U_y$  and  $U_z$  are the displacements imposed to the rigid grips to apply an external mechanical load to the internal crack.

the Al–Al part is the Mishin potential [28], the Al–H part is an upgrade of the potential presented in [29], full details can be found in [30]. The quantities considered for the fitting of the potential are listed below together with the values given by the potential. The reference values, from DFT are given in the next paragraph. The preferred bulk site is the tetrahedral interstitial site (T), with an energy difference between octahedral (O) and tetrahedral (T) of  $\Delta E_{O-T} = 0.147$  eV. A vacancy contains multiple trap sites: 8 tetrahedral ( $T_1$ ) and 6 octahedral ( $O_1$ ) sites.  $T_1$  is the preferred position ( $\Delta E_{seg}^v = -0.3$  eV). The centre of the vacancy is an unstable position for H. The bulk migration barrier is 0.2 eV for a jump from a T site towards an O site. Surface segregation on the  $\{111\}$  surface, in the “threefold” configuration, is -0.46 eV. In addition, a constraint to destabilise the “on top” position was added in the fitting procedure such that it is metastable with a segregation energy of +0.36 eV. The H–H interaction is fitted to reproduce the effective pair interactions between some sites in a grain boundary [30]. It is repulsive.

The corresponding values given by the *ab initio* calculations from the literature are listed below. The energy difference between H in octahedral position and tetrahedral position is  $\delta E_{O-T} = +0.02$  eV (+0.13 eV) [31] with (without) zero point energy correction. The segregation energy in off-centred tetrahedral position in a vacancy is -0.33 eV (without ZPE) [31] and +0.46 eV in the centre of the vacancy [32]. The  $\{111\}$  surface segregation energy is -0.35 eV [5] and the activation energy for bulk diffusion is 0.18 eV (0.15 eV without ZPE) [31].

Quenched Molecular Dynamics (QMD) is used to optimise the system structure. The equations of motion are integrated with a Verlet algorithm, but the velocities are set to 0 when  $\sum_i \vec{f}_i \cdot \vec{v} < 0$ . QMD is run until the maximum force is at least lower than  $10^{-3}$  eV/Å. The crack is loaded quasi-statically. The stress fields after the minimisation are computed from the virial stress tensor. A displacement  $U_z$  is first applied, when the system is relaxed, the value of  $k_I$  is extracted from the  $T_{zz}$  traction profile along the crack plane by a fit to an analytical solution (see details in [26]). Then the crack is loaded in mode II. Increasing values of  $U_y$  are applied which lead, after minimisation, to  $k_{II}$  fields of increasing intensity superimposed to the  $k_I$

fields.  $k_{II}$  is extracted from the  $T_{yz}$  traction profile along the crack plane. It is the specificity of the crack plane orientation ( $\theta = 0$ ) that mode I does not induce any shear load that superposes to the  $T_{yz}$  profile induced by the mode II and vice versa, mode II does not create any opening traction along the crack plane. Then, the crack tip morphology is inspected. Dislocations are detected by their plastic displacement fields: they induce displacement discontinuities ( $\Delta u_x, \Delta u_y, \Delta u_z$ ) across their glide plane.  $\Delta u$  is the difference of the displacement field just above the glide plane, and just below. In the  $k_I, k_{II}$  space, two different events can occur [26]. At high values of  $k_I$ , a Shockley partial dislocation is emitted at an angle of approximately  $70^\circ$  from the crack plane, on the  $\{111\}$  plane that intersects the crack front (the crack front is the intersect). Adding  $k_{II}$  decreases the critical  $k_I$  value for emission ( $k_{Ie}$ ). At moderate and low  $k_I$  values, partial Shockley dislocations are emitted in the crack plane. The simulations in [26] show that  $k_I$  should be lower than approximately  $2/3$  of  $k_{Ie}$  in the absence of mode II if emission along the crack plane is wanted. Once the value of  $k_I$  is fixed, a set of calculations at increasing values of  $k_{II}$  is performed, until the critical value  $k_{IIe}(k_I)$  is reached and the dislocation is emitted.  $\Delta u_z$  is measured at the crack tip at the load immediately below  $k_{IIe}(k_I)$ . It is used in the calculation of  $\gamma_{us}$  to account for the effect of mode I and H, since a part of  $\Delta u_z$  also comes from the relaxations related to the presence of H, as will be shown below.

## 2.2. DFT calculation set-up

The final generalised stacking fault (GSF) energy calculations are done with DFT. They are performed with the VASP (Vienna Ab-initio Simulation Package) implementation [33–35]. The Perdew-Burke-Ernzerhof (PBE) [36] exchange-correlation functional for the generalised-gradient-approximation (GGA) is used. A plane-wave basis set is employed within the framework of the projector augmented wave (PAW) [37] method. On the basis of our tests, we have determined that a cutoff energy of 400 eV and a dense Monkhorst-Pack mesh [38] ( $24 \times 24 \times 24$  k mesh for the primitive cell to sample the Brillouin zone), are adequate for a good convergence. The equilibrium theoretical lattice structure are determined by minimising the Hellmann-Feynman force on the atoms and stress on the unit cell. The convergence of force are set to  $1.0 \times 10^{-3}$  eV/Å, respectively. Ground states properties of fcc-Al, H<sub>2</sub> and Al-H system are thus found in excellent agreement with the literature [31].

We calculate the GSF energy along the  $[11\bar{2}]$  direction on the closed-packed (111) surface along which the glide is the easiest in fcc metals. To simulate the block shearing process we use a slab consisting of 8 atomic layers in the  $[111]$  direction. A large vacuum space of 8 atomic layers parallel to (111) plane are added between the periodically repeated slabs to avoid the interactions between two successive slabs. The top 4 atomic layers of the system are then sheared against the remaining 4 layers on the (111) plane in  $[11\bar{2}]$  direction. For the case of pure Al, each layer of the simulation box contains only one atom. The slide process is rigid. Tests with 12 atomic layers are performed to examine the vacuum effect, and the results of the GSF energy shows no obvious difference.

The effect of H on the GSF energy is investigated by inserting H atoms at high symmetry sites on the glide plane. As in the Rice model the shearing process is rigid, the full atom relaxations is thus not allowed. However, the EAM potential calculations show that the hydrogen introduction at the crack tip have important effect on the relaxation of its neighbour atoms within a certain range. In addition, DFT calcu-

lations [31] show that, in Al, the relaxation invert the stability of the octahedral and tetrahedral sites. Hence, a local relaxation is requested for the hydrogen neighbour atoms within the same range (i.e. the first nearest neighbours) in the GSF energy calculations, the others are kept rigid. Therefore, a much larger simulation box (16 atoms per layer) is used when H atoms are included. To account for the effect of mode I and H on the crack tip behaviours, a displacement  $\Delta u_z$  lower than  $0.08 a_0$  is imposed perpendicular to the shearing plane.

Similar calculations of GSF are also performed with same relaxation criteria but with a much larger box (30 atomic layers and 192 atoms per layer) with the EAM potential. The results are compared to those obtained by.

### 3. Crack Simulations: Results and Analysis

In this section, dedicated to crack simulations, we start with the pure metal case. The outputs are the measures of  $k_{IIe}$  and the crack opening profile. We recall that the "opening" is  $\Delta u_z(y) = (u_z^+ - u_z^-)(y)$ , where  $u_z^+$  (resp.  $u_z^-$ ) is the displacement in the z direction of the atoms of the upper (resp. lower) plane, in first neighbour of the glide plane. Then, the influence of a full line of H on dislocation emission is studied, as a function of the position of the line. The results (the numerical values of  $k_{IIe}(k_I)$ ) are qualitatively analysed by inspecting the H induced displacement field in the vicinity of the crack tip. This profile exhibits a number of features during dislocation emission. The essential information is the value of  $\Delta u_z$  at the corner of the crack, i.e. on the first pair of atoms sheared by the dislocation formation process. It is this value that will be used for the calculation of the GSF in section 4. The justification of the interest of  $\Delta u_z$  at this particular location appears when the match between the  $\gamma_{us}$  values, transformed into  $k_{IIe}$  values by the Rice model, and the brute force QMD results detailed in this section is established. This is postponed until section 4.

#### 3.1. Mixed mode effect on $k_{IIe}$ : the pure metal case

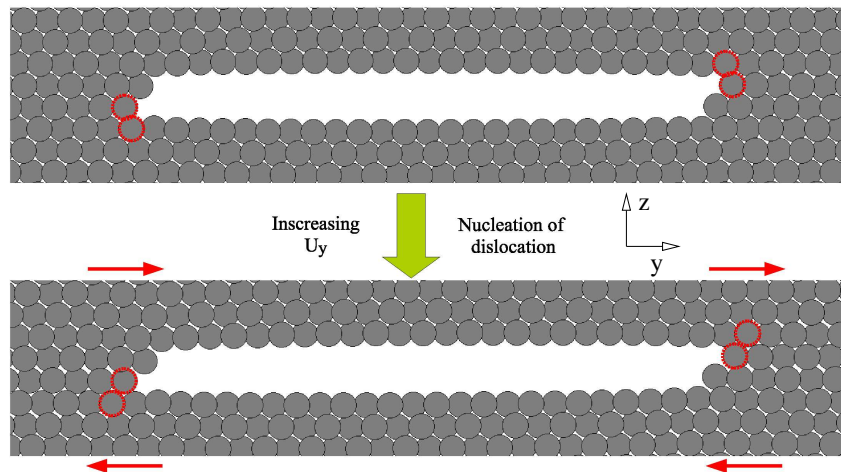


**Figure 2.** Crack configurations before and after the dislocation emission on the crack plane. The plastic shear is highlighted by the atom pairs in dotted lines.



The case of the pure metal is first studied. The critical load  $k_{Ie}$  in pure mode I for the studied configuration of the crack tip is measured, in the case where the dislocation emits at an angle of approximately  $70^\circ$  from the crack plane.  $k_{Ie}$  is about  $0.253 MPa\sqrt{m}$ . For mixed mode loads, three values of  $k_I$  are adopted from the very small one to the one close to  $2/3k_{Ie}$ : 0.045, 0.099 and  $0.187 MPa\sqrt{m}$ , so that dislocation emission occurs in the crack plane. For each fixed  $k_I$ , a set of simulations is run with increasing mode II loads until a Shockley partial dislocation is emitted from both crack tips (see Fig. 2). The atom displacement profiles at the crack tip ( $\Delta u_y$  and  $\Delta u_z$ ) during such an event, are presented in Fig 3.  $\Delta u_y(y) = \Delta u_y^+(y) - \Delta u_y^-(y)$  is the profile of the difference in displacement in the  $y$  direction between the atomic planes above and below the crack plane. The  $\Delta u_y$  profiles, just before the nucleation of dislocation, is presented in Fig. 3(a). It exhibits a singularity due to the presence of the crack. Similar  $\Delta u_y(y)$  are obtained for different mode I loads. In the case of  $k_I = 0.045 MPa\sqrt{m}$ , the time evolution of the  $\Delta u_y$  profile is given (Fig. 3(b)), as a function of the QMD step, at  $k_{IIe}$ . The sequence shows the gradual formation of the Shockley partial and its movement away from the tip. The Shockley partial is fully formed at relaxation step 120 where a step is formed at the tip corresponding to a magnitude of shear of  $0.4 a_0$  (equals to the norm of the Burgers vector  $1/6[112]$ ). It propagates continuously at the right of the crack tip for step numbers larger than 120.

Before the nucleation of the partial, the corresponding profile of  $\Delta u_z$  (labeled  $k_{IIe}^-$  on Fig. 3(c)) is a monotonic decreasing function of  $y$ , with a maximum value of  $0.012 a_0$  at the crack tip. The crack tip is the "corner" of the crack, as shown by the underlined particles on Fig. 2. It is this value which is used for the  $\gamma_{us}$  calculation. Figure 3(d) gathers all the relevant values of  $\Delta u_z$ . Furthermore, when the partial dislocation forms and propagates,  $\Delta u_z$  increases enormously. Especially, when atoms shear ( $\Delta u_y$  on Fig. 3(b)) at about  $0.31$  or  $0.37 a_0$ , the corresponding  $\Delta u_z$  exhibits a maximum. It indicates that the unstable stacking fault may be located in between the shears of  $0.31$  and  $0.37 a_0$ . This demonstrates that in addition to the tensile mode, the shear mode also contributes to the opening of the crack tip when the incipient dislocation is already present. The opening displacements  $\Delta u_z(k_{IIe}^-)$  under critical loads just before the nucleation of the partial (i.e.  $\Delta u_z$  at the corner of the crack) are given in Fig. 3(d) in pure mode I and in mixed mode loading. For both cases, the opening of the crack tip is increased by the superimposed mode I. Besides,  $\Delta u_z$  for mixed mode loads is nearly shifted by a constant amount relative to the values obtained in pure mode I.

The critical mode II stress intensity factor  $k_{IIe}$  for each  $k_I$  are given in Tab. 1. Clearly, mode I decreases  $k_{IIe}$  as the mode I increases the interplanar spacing (see Fig. 3(d)) and thus weakens the atomic bond in between atoms on the two sides of the crack plane, consequently making the shear easier. The quantification of this effect is linked to the gamma surface, and will be presented in Sec. 4.

### 3.2. H effect on the crack tip behaviour

H occupies the tetrahedral interstitial site in fcc Al [31], and the hydrostatic stress around the crack tip in mode I involves a H segregation around the tip. To investigate the maximum effect of H on the crack tip behaviour, we insert a full H line along the crack front on tetrahedral sites around the right crack tip, more specifically where slip localisation occurs, and carry QMD simulations at increasing loads until dislocation emission is observed. Two different crack tips in the system allows for a direct detection

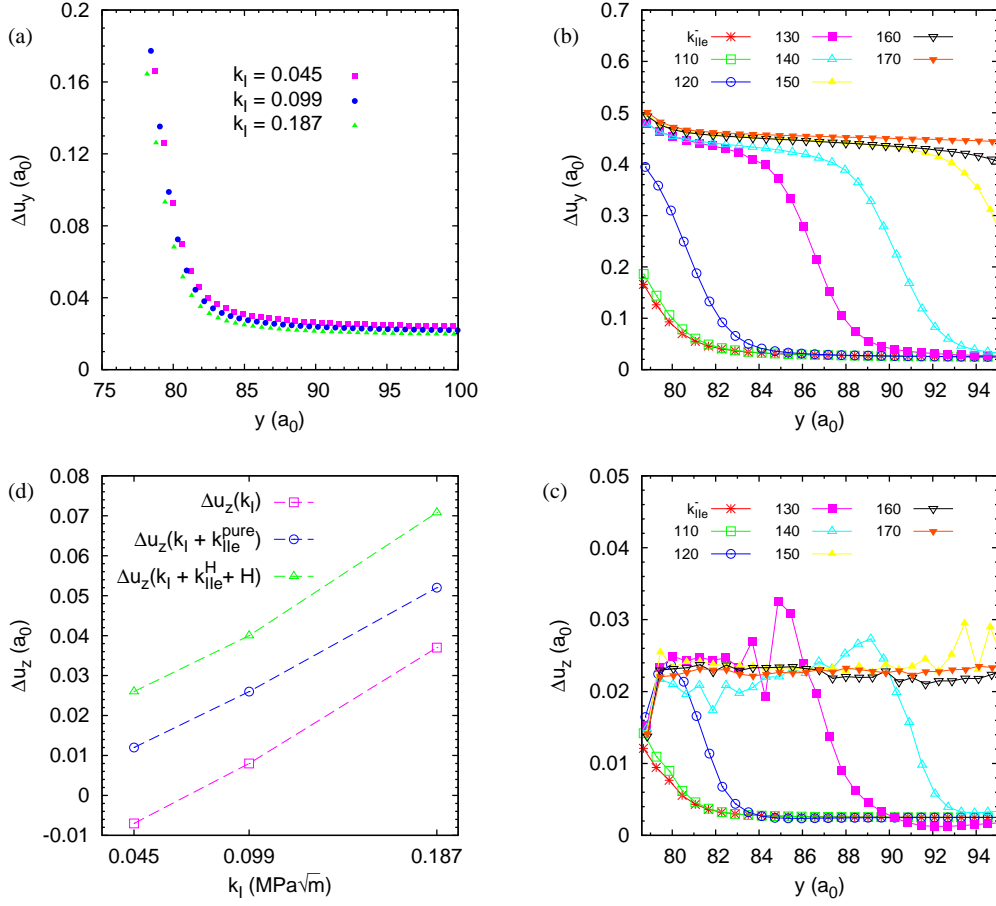


**Figure 3.** (a) Horizontal displacement  $\Delta u_y$  as a function of the  $y$  position for crack tips under critical load just before dislocation emission. (b) Horizontal and (c) vertical displacement ( $\Delta u_y$ ,  $\Delta u_z$ ) as a function of the  $y$  position during the nucleation of Shockley partial dislocations, for the case of  $k_I = 0.045$  MPa $\sqrt{m}$  in mixed modes. (d) Increase of the crack tip opening for crack tips under critical loads of pure mode I, mixed modes, and mixed modes with H (full line in position 3).

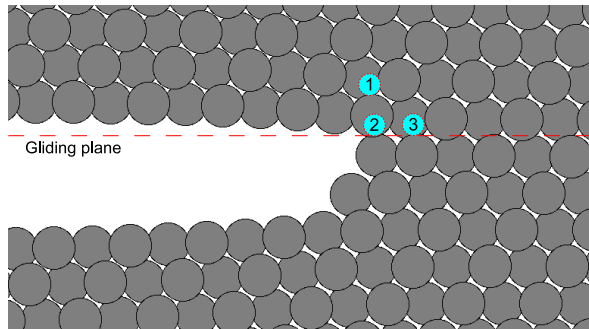


**Figure 4.** Schematic of the crack tip at the right side, with marked tetrahedral positions (blue balls) for the insertion of H.

**Table 1.** Results of the crack simulations, using the EAM potential in [30], under mixed mode I and mode II load.  $k$  units are in  $MPa\sqrt{m}$ .

	Impurity site	$k_{IIe}$	H effect
$k_I = 0.045$	Pure Al	0.123	
	Site 1	0.115	-6.8%
	Site 2	0.102	-17.0%
	Site 3	0.127	+3.3%
$k_I = 0.099$	Pure Al	0.115	
	Site 1	0.104	-9.9%
	Site 2	0.102	-11.0%
	Site 3	0.119	+3.5%
$k_I = 0.187$	Pure Al	0.107	
	Site 1	0.096	-10.0%
	Site 2	*	*
	Site 3	0.116	+8.4%

\*The dislocation is emitted on another plane.

of an enhancement or blocking of dislocation emission. However, if H impedes emission and emission occurs on the other crack tip, another H line is inserted on the symmetric site of the left crack tip. Then the load is increased further until  $k_{IIe}$  is reached. Three interstitial sites showed in Fig. 4 are examined. The corresponding  $k_{IIe}$  are measured and presented in Tab. 1. The H induced atomic displacement field around the crack tip are also presented in Fig. 5. The displacement map is built from two separate simulations: one with H and another one without H, both with the same applied mechanical load.

First we consider H on position 1 (Fig. 4). It leads to a weak decrease of  $k_{IIe}$ . The increasing mode I load enhances this effect (Tab. 1). This crack tip shielding can be partly attributed to the elastic effect induced by H [39]. From the displacement field (Fig. 5(a)) we can see that H on position 1 involves a dilatation, which helps the relative displacements between atoms above and below the crack plane on the right hand of H. These displacements enhance the shear discontinuity in between the three rows of atoms below and above the glide plane.

H on position 2 induces a more significant reduction in  $k_{IIe}$  (Tab. 1). Mode I decreases this effect. Position 2 becomes unstable upon shearing (within the limitations of the EAM potential). The displacement field relevant to the very beginning of atom relaxation is shown in Fig. 5(b). The empty red circle represents the initial position 2 and the filled circle represents the relaxed position: H relaxes from position 2 towards a surface site. Furthermore, H attracts the 2 Al atoms at the corner of the tip. The right top atoms seem to be repelled by H, while those at the right bottom are attracted. The crack tip is therefore already sheared by the presence of H. The displacement field after full relaxation is presented in Fig. 5(c). Obviously the dislocation was emitted. It propagated until it reached an equilibrium with the stacking fault force.

H on position 3 slightly increases  $k_{IIe}$ , and mode I load amplifies this effect (Tab. 1). From the corresponding displacement field (Fig. 5(d)) it is hard to know how H impacts the shear process : it stretches the Al-Al bonds in first neighbour position, induces a shear at the crack tip and furthermore one can also expect a higher resistance to shear because of the compression of the Al-H bond. Indeed the final analysis, from the GSF, at the end of section 4.2 will show that the apparent increase of  $k_{IIe}$  is, in fact, the result of a compensation in between all these effects. However, it is noted that H in this position strongly repels its first shell of neighbours, which should be considered in the simulation of the shear process in  $\gamma_{us}$  calculations. Figure 6(a) presents  $\Delta u_y$  profile

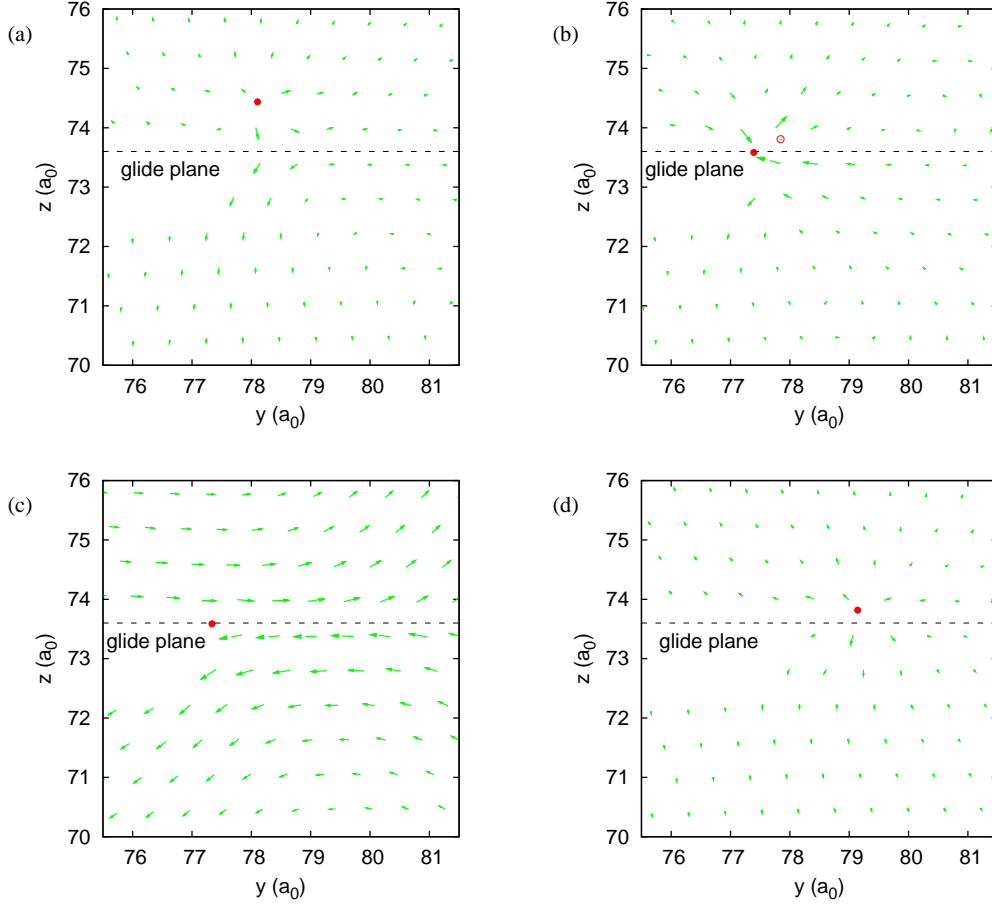


**Figure 5.** (a) Projected atomic displacement field on the  $(1\bar{1}0)$  plane, induced by the presence of the H line on position 1. The starting point of the vectors are the relaxed positions without H, while the end of the vectors is the relaxed positions in the presence of H. The vector length is enlarged by a factor of 5. The red filled circle is the relaxed H position. The crack tip is under mixed loads where  $k_I = 0.099 \text{ MPa}\sqrt{\text{m}}$ . (b) Projected atomic displacement field relevant to the very beginning of the relaxation when H occupies position 2 (red empty circle). (c) Projected atomic displacement after full relaxation when H occupies position 2. (d) Projected atomic displacement field when H occupies position 3.

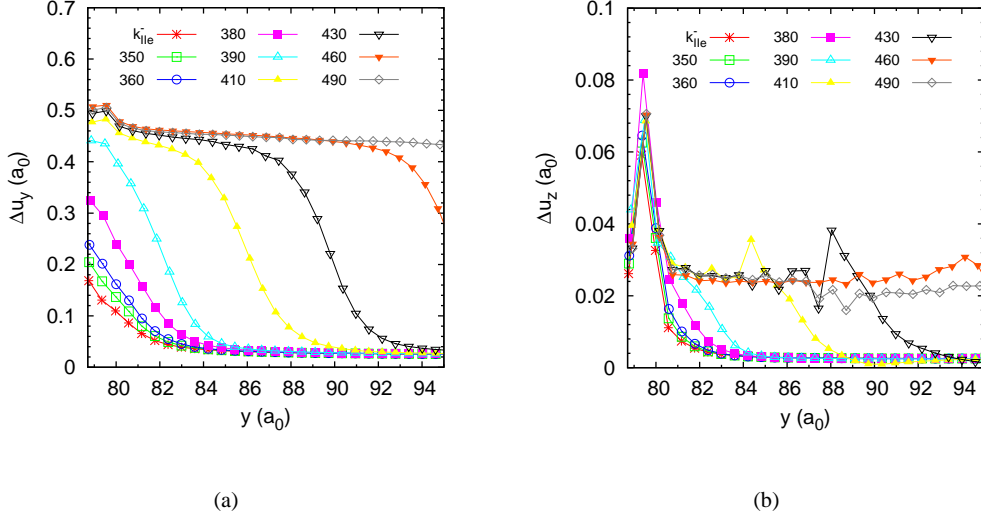


**Figure 6.** (a) Horizontal and (b) vertical displacement as a function of the  $y$  position during the nucleation of Shockley partial dislocations. The profiles labeled  $k_{IIe}^-$  correspond to a mechanical load just below the one for dislocation emission.

in this case (H on position 3) during dislocation emission. After the full formation of the partial dislocation (from relaxation step 390), a small hump appears on the  $\Delta u_y$  curve at  $y=79.5 a_0$ , where H is located. It means that H enhances shear localisation after the full formation of the partial. The  $\Delta u_z$  profile in Fig. 6(b) shows that H very significantly increases  $\Delta u_z$  around it and helps open the crack tip. The H induced increase of crack tip opening  $\Delta u_z$  is compared to that of pure metal case in Fig. 3(d). H enlarges the crack tip opening by 0.015 to 0.02  $a_0$ , and this shift is almost constant with  $k_I$ .

#### 4. H effect on the generalised stacking fault energy

In a previous paper [40], we have shown precisely how the interstitial sites in the glide plane are deformed during the shear process and the consequences on the stability of H. Both EAM and DFT calculations show that the tetrahedral sites of the glide plane are continuously transformed in the octahedral site of the intrinsic stacking fault ( $O_{ISF}$ ). In DFT,  $O_{ISF}$  is the most stable site of the stacking fault, while in EAM, the tetrahedral site is always preferred. However, no site change was found in EAM during the shearing process when the hydrogen is initially in sub-surface position 3.

##### 4.1. Details about the relaxations

In the following, we review the various methods used in the literature for relaxing the H environment during the GSF calculation. Since our work does not show the same trend as the ones reported before, we have reproduced some of the results of the literature. It demonstrates the impact of relaxations. We start first by the case of pure Al and precisely quantify the effect of the opening perpendicular to the glide plane. Then we detail the results obtained with the EAM calculations and precisely establish the link between the method used for the GSF calculation (opening and H

concentration) and the data collected at the crack tip from QMD simulations. Finally the method is used in DFT and the conclusions concerning the effect of sub-surface H on dislocation emission are exposed.

We have used three different ways to calculate the energy landscape associated with glide. First, in the pure metal case, the atoms are not relaxed. The GSF is simply obtained by a rigid blocks shearing. The opening  $\Delta u_z$  is applied by translating one block with respect to the other in the z direction. The second method is the one used by Gang Lu [41] where: the H environment is first fully relaxed (at zero shear), the two blocks are rigidly sheared,  $\Delta u_z$  is applied and only the atoms in the first planes above and below the glide plane are relaxed, in the z direction only. It means that the transversal relaxations around the H atom, inherited from the initial relaxation, are held fixed during the calculation of the whole GSF. This method is referred to as ZR for “relaxations in z direction” in the next sections. In the third method, only the neighbours of H within a radius of  $0.74 a_0$  are relaxed (it is enough to recover most of the effect on the relative stability of the T and O site),  $\Delta u_z$  is applied and the first neighbours and the H atoms are relaxed at every step. If H occupies the T+ site, the number of relaxed atoms is 4 and it goes up to 8 during the shear. This method is called LR for “local relaxations”.

#### 4.2. Results obtained with the EAM potential

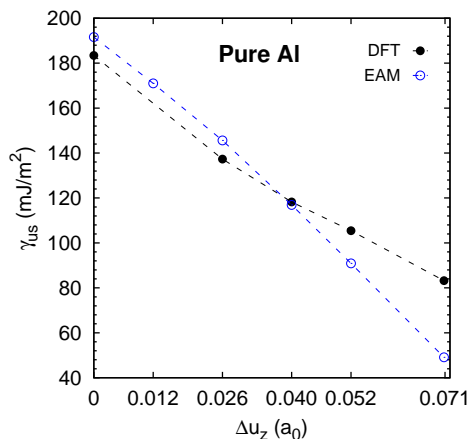


**Figure 7.** EAM and DFT computed unstable stacking fault energy as a function of  $\Delta u_z$  in the pure Al.

The unstable stacking energy ( $\gamma_{us}$ ), in the pure metal, decreases strongly with  $\Delta u_z$  (Fig. 7). It is cut down by almost 50% for a value of  $\Delta u_z$  of the order of  $0.05 a_0$  which is representative of the crack tip loaded at a moderate mode I: it can be checked on Fig. 3(d) that this level of opening corresponds to a mixed mode loading with  $k_I$  of  $0.187 \text{ MPa}\sqrt{m}$ . The agreement between DFT and EAM is good (Fig. 7). Figure 8 shows the rigid GSF for three values of  $\Delta u_z$ . We can note that the maximum energy ( $\gamma_{us}$ ) is not obtained at  $0.5 b$ , but in between  $0.6 b$  and  $0.7 b$ . This confirms that, when H is introduced in the calculation, it will make the transition towards the sites of the hcp structure, before  $\gamma_{us}$  is reached, as discussed above. The agreement between Rice’s model and the  $k_{Ile}$  measured at the crack tip, for pure Al, is good. It can be seen in Tab. 2 by comparing the column “EAM potential”, which contains the values

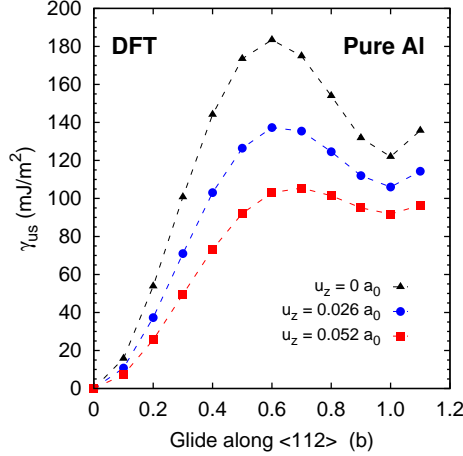


**Figure 8.** Generalised stacking fault energies as function of a shear along the  $\langle 112 \rangle$  direction are computed in pure Al for different values of  $\Delta u_z$ .

obtained by brute force QMD, with the column “Rice (EAM)”, which contains the  $k_{IIe}$  values calculated from  $\gamma_{us}$  using Eq. 1, with the opening from Fig.3(d) (curve  $\Delta u_z(k_I + k_{IIe}^{pure})$ ). This agreement is well in line with what is published in [26], but with a different crack tip (the crack was built by removing a single layer of Al). It also confirms that the location where  $\Delta u_z$  is measured, i.e. at the crack corner in between the pair of atoms that are the first to be sheared, is appropriate and that the model captures the effect mode I loading.

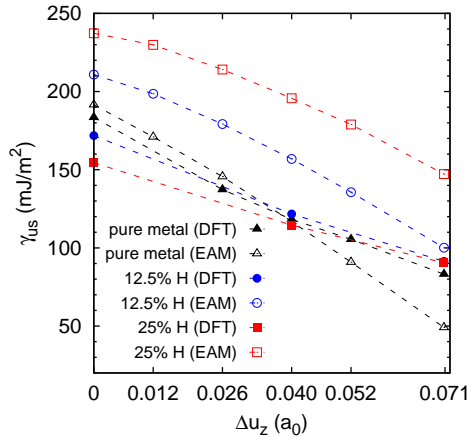


**Figure 9.** Variation of  $\gamma_{us}$  as a function  $\Delta u_z$  (the opening) for different levels of H coverage, in EAM and in DFT.

The next issue is how much hydrogen should be introduced in the GSF calculation in order to mimic what occurs at the crack tip. A natural choice would be 100%, since a full line is introduced. However, site 3 is not at the tip, but at the level of the second row of atoms along the glide plane (Fig. 4). Furthermore, we know that it has a strong impact on the relaxation of its first neighbours. Therefore, we can expect that the H line has an influence on the rising slip distribution over a wide range. In developing Eq. 1, Rice (equation 11 in [24]) uses the J integral for a contour along the glide plane,

**Table 2.**  $k_{IIe}$  values (in  $MPa\sqrt{m}$ ) obtained by brute force QMD simulations using the EAM potential (column "EAM potential") and one line of H on site 3, tabulated using the Rice formula Eq. 1 from  $\gamma_{us}$  calculated by EAM (column "Rice (EAM)") or by DFT (column "Rice (DFT)") with a surface coverage of 12.5% H (see text).

	Impurity site	EAM Potential		Rice (EAM)		Rice (DFT)	
		$k_{IIe}$	H effect	$k_{IIe}(\gamma_{US})$	H effect	$k_{IIe}(\gamma_{US})$	H effect
$k_I = 0.045$	Pure Al	0.123		0.127			
	Site 3	0.127	3.3%	0.130	2.4%		
$k_I = 0.099$	Pure Al	0.115		0.117		0.114	
	Site 3	0.119	3.5%	0.122	3.6%	0.107	-5.9%
$k_I = 0.187$	Pure Al	0.107		0.093		0.100	
	Site 3	0.116	8.4%	0.098	5.6%	0.093	-7.0%

which gives:

$$J = - \int_0^{\infty} \tau \partial \delta / \partial x_1 dx_1 \quad (3)$$

where  $\tau$  is the shear stress along the glide plane. It is a function of  $x_1$ , the distance along the glide plane. Since he considers only static mechanical equilibrium, this shear stress is also related to the slip discontinuity profile, via the non linear stress / slip discontinuity relation, which is the gamma surface. Noting that  $\tau(x_1)$  is, in the case where the slip plane has uniform physical properties,  $\tau(\delta(x_1))$ , Eq. 3 can be rewritten:

$$J = - \int_0^{\infty} \tau \partial \delta / \partial x_1 dx_1 = \int_0^{\delta_{tip}} \tau d\delta = \Phi(\delta_{tip}) \quad (4)$$

where  $\delta_{tip}$  is the displacement discontinuity at the crack tip ( $x_1 = 0$ ). When the mechanical load on the crack tip reaches  $k_{IIe}$ ,  $\Phi(\delta_{tip})$  is  $\gamma_{us}$ . The step from Eq. 3 to Eq. 4 relies on the uniform property of the glide plane over the region where the slip distribution rises. It is not the case in the presence of the line of H. We expect  $\tau(\delta)$  to vary depending on the distance to the line of hydrogen atoms. To turn around this difficulty, we consider that H uniformly affects the  $\tau(\delta)$  relation and we evaluate it by inserting a line of H in the simulation box used for the GSF calculation. Various H densities have been tested: 25% (one row of H for 4 rows of Al in the glide plane) and 12.5% (8 rows of Al). With the EAM potential, H increases considerably the unstable stacking energy, as seen on Fig. 9 by comparing the values for different H coverage and a single  $\Delta u_z$  value. Nevertheless, this effect is damped by the impact of H on  $\Delta u_z$ , i.e., from figure 3(d) we know that the full line of H, introduced on site 3, increases the opening at the crack tip. This, in turn, decreases  $\gamma_{us}$  (Fig. 9) and the two effects compensate. Again, the comparison of columns "EAM Potential" and "Rice (EAM)" in Tab. 2, show that a reasonable agreement can be found. This was obtained by taking a concentration of 12.5%H (25% gives a much too strong increase of  $k_{IIe}$  in comparison to the QMD results). This means that 1 line of H was introduced in the GSF calculation for every 8 Al rows. These 8 rows roughly correspond to the size of the core of the partial dislocation as seen on the slip distributions on Fig. 3(b), which is coherent.

In a recent paper [42], some crack simulations were done which show no effect of mode I in Cu and Ni. The data in Al (Fig. 12 of [42], before emission occurs in a different plane than at low mode I) is coherent with table 1, in the sense that



a moderate decrease is observed, of the order of 10%, even if the crack tip has a different shape than the one considered here. Concerning the absence of effect in Cu and Ni, their enthalpy calculations show indeed that the decrease in  $\gamma_{us}^{enthalpy}$  due to a transverse traction is lower in Cu and Ni than in Al, so maybe this is the reason why the effect does not show up in the simulations in Cu and Ni. Furthermore, in the simulations, the crack tip geometry is such that there is a change of the surface during dislocation emission (in contrast to an atomistically sharp crack of the same orientation) and this might also influence the value of  $k_{IIe}$  with unknown effects from  $k_I$ .

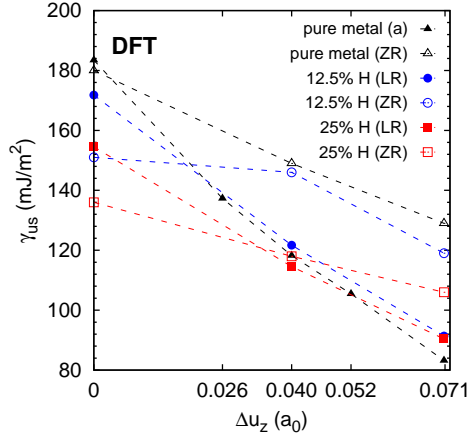


**Figure 10.** Variation of  $\gamma_{us}$  as a function  $\Delta u_z$  (the opening) for different H coverage and different relaxation methods in DFT. ZR refers to relaxations in z only of the Al toms of the two first layers around the glide plane. LR refers to a local relaxation where Al atoms within a sphere of  $0.73 a_0$ .

### 4.3. Results obtained from DFT

Finally, we use DFT to evaluate the effect of H on the GSF, with the  $\Delta u_z$  range taken from the EAM simulations. Different relaxation methods give different trends. We have compared relaxations in the z direction, limited to the layers in first neighbour position of the glide plane, with local relaxations, labeled respectively ZR and LR in Fig. 10 (see section 4.1). The ZR method shows a clear trend: H always reduces  $\gamma_{us}$ , whatever the value of  $\Delta u_z$ , and the effect increases with increasing H coverage. Here the coverage is a little different from EAM because of system size constraints. The concentration 12.5% is obtained by putting half a line of H every 4 rows of Al. On the contrary, the LR method shows a reduction of  $\gamma_{us}$ , only when the opening in z is zero. For higher values of  $\Delta u_z$ , but still in the range obtained by a mechanical effect only ( $\Delta u_z = 0.05 a_0$  at  $k_I = 0.187 \text{ MPa}\sqrt{m}$  and  $k_{II} = k_{IIe}$ ), H has a negligible effect on  $\gamma_{us}$ . This contradicts the messages (that are contradictory) found in the literature where it can be found that H decreases  $\gamma_{us}$  [41] or prevents glide [43], depending on concentration. Concentrations are much higher than those used in the present work. We can also mention that, as a check, we reproduced the results obtained by G. Lu exactly using the same LDA functional.

When the values obtained by the LR method are introduced in the Rice formula, a decrease of  $k_{IIe}$  is found. This effect is essentially related to the mechanical loading of the crack tip, since the impact on  $\gamma_{us}$  itself is not significant beyond  $\Delta u_z = 0.04 a_0$ . If

the predictions from the EAM on the influence of H on  $\Delta u_z$  are taken into account, an extra decrease of  $k_{IIe}$  is obtained (table 2, last column). Knowing that the EAM gives an increase in  $\gamma_{us}$ , which is opposite to the DFT results, this effect might not be realistic. Indeed, by construction, this EAM treats the Al-H bond as a short range pair repulsion in the bulk (the non linear embedding functional is used to handle the segregation of H to open structures like vacancies or surfaces), following the appealing picture for H in metals given by the early Effective Medium Theory [30, 44]. Upon shearing, the H atom is pushed from the atomic environment of a tetrahedral site of the fcc structure (T) to an octahedral site of the hcp structure (O hcp) [40]. In the undistorted fcc, the EAM was fitted to give an energy for H in the O site 0.15 eV higher than in the T site (which is the case in DFT, but without ZPE). In DFT, the two positions have almost the same energy when the zero point energy correction is taken into account [31]. Adding the ZPE to the values used for fitting the potential does not have any physical meaning and therefore was not done. The effect of a rigid block shearing on the segregation energy of H ( $\Delta E_{seg}$ ) to the glide plane was quantified in [40] (Fig. 4a with  $\Delta u_z = 0$  and Fig. 4b with  $\Delta u_z = 0.05 a_0$ , curve T+  $\rightarrow$  O (hcp)). An increase of the segregation energy, with glide, explains qualitatively why the EAM gives an increase in  $\gamma_{us}$ . Especially when  $\Delta u_z = 0.05 a_0$ , the segregation is very low (-0.25 eV) in the absence of glide. This comes from the fitting of the segregation energy to open structures (vacancies and surfaces), which is low. Then the distortion of the T site with glide leads to a steep increase in  $\Delta E_{seg}$  [40]. This shows that the effect of H on  $\gamma_{us}$  is deeply rooted in the potential, i.e. not only in the simple repulsive pair part, and therefore difficult to correct: having a weak effect of  $\Delta u_z$  on the segregation energy and, at the same time, a strong decrease of  $\Delta E_{seg}$  at surfaces seems opposite. An interest of the present DFT calculations is also to be used as a benchmark to evaluate the limits of the EAM potential.

It is therefore likely, but not proved, that we overestimate the effect of H on  $\gamma_{us}$  if we take into account the influence of H on  $\Delta u_z$  given by the EAM at the crack tip. A conservative approach is to ignore it and consider only the effect of the mechanical load on  $\Delta u_z$ . Then the essential results from DFT are:

- The first order effect on  $k_{IIe}$  comes from the mode I loading, i.e. that an opening mechanical load perpendicular to the glide plane can decrease  $\gamma_{us}$  by 40%, i.e. decrease  $k_{IIe}$  by 25%, for small values of  $k_I \sim 0.2 MPa\sqrt{m}$  ( $\Delta u_z \sim 0.05 a_0$  implies a drop of  $\gamma_{us}$  from 180 to 105 mJ/m<sup>2</sup>).
- In comparison, H has a small effect, even for very large concentrations on the glide plane. For realistic concentrations, the effect is expected to be negligible, in Al.

## 5. Conclusion

In this paper, we have studied the impact of sub-surface H and of mixed mode loading on dislocation emission. Multiple methods were used combining EAM and DFT, crack simulations, GSF calculations and Rice's model.

First, in the pure metal case, we found a strong effect of transverse mechanical load on  $k_{IIe}$  measured directly by crack simulations, confirmed by  $\gamma_{us}$  calculations by EAM and DFT. Up to 25% decrease in  $k_{IIe}$  can be expected from Rice's model considering  $\gamma_{us}$  decreases from 180 to 105 mJ/m<sup>2</sup> (from the DFT data in Fig. 7). The effect of mode I is limited because a too high traction will induce emission out of the

crack plane. Second, the H effect was investigated. Using EAM, H slightly increases  $k_{IIe}$  in comparison to  $k_{IIe}$  in pure Al, both at the same  $k_I$ . We have analysed this result by calculating  $\gamma_{us}$  as a function of  $\Delta u_z$  (the crack opening) and H coverage.  $\Delta u_z$  are taken at the crack tip in the presence of H, at  $k_{IIe}^-$ . The H coverage for the GSF calculations, was fixed to 12.5% (1 H line for 8 Al row, in the glide plane) based on a comparison between the crack simulations and the results obtained with Rice’s model. The same methodology was used to calculate  $\gamma_{us}$  by DFT (i.e. local relaxations, low H coverage and  $\Delta u_z$  from crack simulations). The trend, from the DFT data and Rice’s model, is that an decrease of  $\gamma_{us}$  can be expected at low mode I, but the effect becomes negligible beyond  $k_I = 0.1 \text{ MPa}\sqrt{\text{m}}$ . This leads to the conclusion that the strong effect is mechanical (mode I) and sub-surface H influence is negligible.

## Acknowledgments

This work was granted access to the HPC resources of CALMIP (CICT Toulouse, France) under the allocations 2014-p0912 and 2014-p0749. The authors acknowledge the support of the French Agence Nationale de la Recherche (ANR), under grant *EcHyDNA* (Blanc 10-19424).

## References

- [1] R.P. Gangloff, *Hydrogen assisted cracking of high strength alloys*, in *Comprehensive structural integrity*, I. Milne, R.O. Ritchie, and B. Karihaloo, eds. Elsevier Science New York, NY, 2003, pp. 31–101.
- [2] R.P. Gangloff, *H-enhanced deformation and fracture in the crack tip process zone*, in *Materials performance in hydrogen environments (Proceedings of the 2016 International Conference on fracture)*, B.P. Sommerday and P. Sofronis, eds. ASME, 2017, pp. 1–35.
- [3] G.M. Scamans, R. Alani, and P.R. Swann, *Pre-exposure embrittlement and stress corrosion failure in AlZnMg alloys*, *Corrosion Science* 16 (1976), pp. 443–459.
- [4] A. Van der Ven and G. Ceder, *Impurity-induced van der waals transition during decohesion*, *Phys. Rev. B* 67 (2003), p. 060101.
- [5] D. Jiang and E.A. Carter, *First principles assessment of ideal fracture energies of materials with mobile impurities: implications for hydrogen embrittlement of metals*, *Acta Materialia* 52 (2004), pp. 4801 – 4807.
- [6] H. Birnbaum, I. Robertson, P. Sofronis, and D. Teter, *Mechanisms of Hydrogen Related Fracture-A review*, in *Proceedings of CDI’96, Th. Magnin ed., The Institute of Materials*. 1997, p. 172.
- [7] I.M. Robertson, *Hydrogen embrittlement understood*, *Met. Trans. A* 46A (2015), p. 2323.
- [8] I. Aubert, N. Saintier, J.M. Olive, and F. Plessier, *A methodology to obtain data at the slip-band scale from atomic force microscopy observations and crystal plasticity simulations.*, *acta mater.* 104 (2016), pp. 9–17.
- [9] Y. Deng and A. Barnoush, *Hydrogen embrittlement revealed via novel in situ fracture experiments using notched micro-cantilever specimens*, *acta mater* 142 (2018), pp. 236–247.
- [10] S.P. Lynch, *Mechanisms and Kinetics of Environmentally Assisted Cracking: Current Status, Issues, and Suggestions for Further Work*, *Metallurgical and Materials Transactions A* 44 (2013), pp. 1209–1229.
- [11] Y. Fukai and N. Okuma, *Formation of superabundant vacancies in Pd hydride under high hydrogen pressures*, *Phys. Rev. Lett.* 73 (1994), p. 1640.

- [12] M. Nagumo, *Hydrogen related failure of steels a new aspect*, Materials Science and Technology 20 (2004), pp. 940–950.
- [13] D.G. Xie, Z.J. Wang, J. Sun, J. Li, E. Ma, and Z.W. Shan, *In situ study of the initiation of hydrogen bubbles at the aluminium metal/oxide interface*, Nature Materials 14 (2015), p. 899.
- [14] A. Tehranchi and W.A. Curtin, *Atomistic study of hydrogen embrittlement of grain boundaries in nickel: II. decohesion*, Model. Sim. Mat. Sci. Eng. 25 (2017), p. 075013.
- [15] B. Kuhr, D. Farkas, and I.M. Robertson, *Atomistic studies of hydrogen effects on grain boundary structure and deformation response in fcc Ni*, Comp. Mat. Sci. 122 (2016), pp. 92–101.
- [16] D. Tanguy, *Cohesive stress heterogeneities and the transition from intrinsic ductility to brittleness*, Phys. Rev. B 96 (2017), p. 174115.
- [17] T. Miura, K. Fujii, and K. Fukuya, *Micro-mechanical investigation for effects of helium on grain boundary fracture of austenitic stainless steel*, Journal of Nuclear Materials 457 (2015), pp. 279–290.
- [18] S. Li, Y. Li, Y.C. Lo, T. Neeraj, R. Srinivasan, X. Ding, J. Sun, L. Qi, P. Gumbsch, and J. Li, *The interaction of dislocations and hydrogen-vacancy complexes and its importance for deformation-induced proto nano-voids formation in  $\alpha$ -Fe*, International Journal of Plasticity 74 (2015), pp. 175–191.
- [19] A. Tehranchi, X. Zhang, G. Lu, and W.A. Curtin, *Hydrogen-vacancy-dislocation interactions in  $\alpha$ -Fe*, Modelling Simul. Mater. Sci. Eng. 25 (2017), p. 025001.
- [20] J. Song and W. Curtin, *Mechanisms of hydrogen-enhanced localized plasticity: An atomistic study using  $\alpha$ -Fe as a model system*, Acta Materialia 68 (2014), pp. 61 – 69.
- [21] Y. Sun, Q. Peng, and G. Lu, *Quantum mechanical modeling of hydrogen assisted cracking in aluminum*, Phys. Rev. B 88 (2013), p. 104109.
- [22] R.J. Zamora, A.K. Nair, R.G. Hennig, and D.H. Warner, *Ab initio prediction of environmental embrittlement at a crack tip in aluminum*, Phys. Rev. B 86 (2012), p. 060101(R).
- [23] D.H. Warner, W.A. Curtin, and S. Qu, *Rate dependence of crack-tip processes predicts twinning trends in f.c.c. metals*, nat. mat. 6 (2007), p. 876.
- [24] J.R. Rice, *Dislocation nucleation from a crack tip: An analysis based on the peierls concept*, Journal of the Mechanics and Physics of Solids 40 (1992), pp. 239–271.
- [25] S.J. Zhou, A.E. Carlsson, and R. Thomson, *Dislocation nucleation and crack stability: Lattice Green’s-function treatment of cracks in a model hexagonal lattice*, Phys. Rev. B 47 (1993), pp. 7710–7719.
- [26] K. Gouriet and D. Tanguy, *Dislocation emission from a crack under mixed mode loading studied by molecular statics*, Philosophical Magazine 92 (2012), pp. 1663–1679.
- [27] D. Tanguy, M. Razafindrazaka, and D. Delafosse, *Multiscale simulation of crack tip shielding by a dislocation*, acta mater. 34 (2008), p. 2441.
- [28] Y. Mishin, D. Farkas, M.J. Mehl, and D.A. Papaconstantopoulos, *Interatomic potentials for monoatomic metals from experimental data and ab initio calculations*, Phys. Rev. B 59 (1999), pp. 3393–3407.
- [29] D. Tanguy and T. Magnin, *Atomic-scale simulation of intergranular segregation of H in AlMg: implications for H-induced damage*, Philosophical Magazine 83 (2003), pp. 3995–4009.
- [30] X. Shen, D. Tanguy, and D. Connétable, *Atomistic modelling of hydrogen segregation to the  $\Sigma 9\{221\}[110]$  symmetric tilt grain boundary in Al*, Philosophical Magazine 94 (2014), pp. 2247–2261.
- [31] C. Wolverton, V. Ozolins, and M. Asta, *Hydrogen in aluminum: First-principles calculations of structure and thermodynamics*, Phys. Rev. B 69 (2004), p. 144109.
- [32] D. Connétable, Y. Wang, and D. Tanguy, *Segregation of hydrogen to defects in nickel using first-principles calculations: The case of self-interstitials and cavities*, Journal of Alloys and Compounds 614 (2014), pp. 211 – 220.
- [33] G. Kresse and J. Hafner, *Ab initio molecular dynamics for liquid metals*, Phys. Rev. B 47 (1993), p. 558.

- [34] G. Kresse and J. Hafner, *Ab initio molecular-dynamics simulation of the liquid-metalamorphous-semiconductor transition in germanium*, Phys. Rev. B 49 (1994), p. 14251.
- [35] G. Kresse and J. Furthmüller, *Efficient iterative schemes for ab initio total-energy calculations using a plane-wave basis set*, Phys. Rev. B 54 (1996), p. 11169.
- [36] J.P. Perdew, K. Burke, and M. Ernzerhof, *Generalized gradient approximation made simple*, Phys. Rev. Lett. 77 (1996), pp. 3865–3868.
- [37] G. Kresse and D. Joubert, *From ultrasoft pseudopotentials to the projector augmented-wave method*, Phys. Rev. B 59 (1999), p. 1758.
- [38] H. Monkhorst and J. Pack, *Special points for brillouin-zone integrations*, Phys. Rev. B 13 (1976), p. 5188.
- [39] J. Weertman and J.E. Hack, *Stress intensity factors for crack tip shielding or anti-shielding by impurity atoms*, International Journal of Fracture 30 (1986), pp. 295–299.
- [40] Y. Wang, D. Connétable, and D. Tanguy, *Site stability and pipe diffusion of hydrogen under localised shear in aluminium*, Phil. Mag. 99 (2019), pp. 1184–1205.
- [41] G. Lu, D. Orlikowski, I. Park, O. Politano, and E. Kaxiras, *Energetics of hydrogen impurities in aluminum and their effect on mechanical properties*, Phys. Rev. B 65 (2002), p. 064102.
- [42] P. Andric, B. Yin, and W.A. Curtin, *Stress-dependence of generalized stacking fault energies*, JMPS 122 (2019), pp. 262–279.
- [43] F. Apostol and Y. Mishin, *Hydrogen effect on shearing and cleavage of Al: A first-principles study*, Phys. Rev. B 84 (2011), p. 104103.
- [44] J. Nørskov and F. Besenbacher, *Theory of hydrogen interations with metals*, J. Less-Common Metals 130 (1987), pp. 475–490.